Arch. Mech., 33, 5, pp. 717–737, Warszawa 1981

A quest for micropolar elastic constants Part II

R. D. GAUTHIER (GOLDEN) and W. E. JAHSMAN (BOULDER)

EARLIER investigations by the authors attempted by means of static experiments to detect and measure the six elastic constants predicted by the theory of micropolar elasticity in which a specially constructed micropolar material was used. This consisted of aluminum shot embedded in an epoxy matrix. It was concluded that the experiments lacked the necessary resolution to identify any departure from classical elastic behavior. In the present work a Kolsky apparatus is utilized to generate a stress wave which propagates axially through a short cylindrical specimen of the same material. To assist in the interpretation of the experimental data, an analogous analysis of the Rayleigh-Lamb infinite plate problem in plane strain was made in which the constitutive equations of micropolar elasticity were inserted. Dispersion relations were derived and curves which compare micropolar and classical behavior were generated from the solution. An additional wave equation was found which pertains strictly to microrotational modes and is not a part of the classical Rayleigh-Lamb theory. These modes appeared as unique ripple frequencies. From these waves, superposed on the normal singnals, two micropolar wave speeds are concluded and two of the six micropolar moduli for this special material are determined. Two others are found from static tests. It is concluded that micropolar waves can be excited and detected in a dynamic experiment of this type.

W swych poprzednich pracach autorzy stosując doświadczenia statyczne starali się wykryć i zmierzyć sześć stałych sprężystości przewidzianych teorią specjalnie skonstruowanego materiału mikropolarnego składającego się ze śrutu aluminiowego, zatopionego w matrycy epoksydowej. Analiza szeregu rozwiązań problemów brzegowych wykazała, że moduły mikrosprężystości można by określić na podstawie odpowiednio dobranych prób rozciągania, skręcania i zginania próbek różnych rozmiarów. Po przeprowadzeniu dużej liczby doświadczeń ustalono jednak, że zdolność rozdzielcza przeprowadzonych doświadczeń jest zbyt mała na to, by stwierdzić tu jakiekolwiek odstępstwa od klasycznych własności sprężystych i nie można w ten sposób ustalić ważności teorii mikropolarnej sprężystości. W niniejszej pracy zastosowano podejście dynamiczne zasugerowane przez posiadaną przez nas aparaturę do badań doświadczalnych. Zastosowano mianowicie aparaturę Kolskiego służącą do generacji fali naprężenia przemieszczającej się osiowo wzdłuż krótkiej próbki cylindrycznej wykonanej z tego samego materiału co materiał użyty wcześniej w doświadczeniach statycznych. Stwierdzono, że w doświadczeniach takich można wytwarzać i wykrywać fale mikropolarne oraz że takie postępowanie stwarza możliwość weryfikacji mikropolarnej teorii sprężystości.

В своих предыдущих работах авторы, применяя статические эксперименты, старались обнаружить и измерить шесть упругих постоянных, предсказываемых теорией специально построенного микрополярного материала, состоящего из алюминиевой дроби погруженной в эпоксидной матрицы. Анализ ряда решений граничных задач показал, что модули микроупругости можна бы определить на основе соответственно подобранных испытаний растяжения, скручивания и изгиба образцов разных размеров. После проведения большого количества экспериментов установлено однако, что разделительная способность проведенных экспериментов слишком мала для того, чтобы констатировать здесь какие-нибудь отступления от классических упругих свойств и нельзя таким образом установить важности теории микрополярной упругости. В настоящей работе применен динамический подход внушенный находящейся у нас аппарамурой для экспериментальных исследований. Именно применена аппаратура Кольского, служащая для генерации волны напряжения, перемещающейся поосно вдоль короткого цилиндрического образца, изготовленного из того же самого материала что материал использованный ранее в статических экспериментах. Констатировано, что в таких экспериментах можно генерировать и обнаруживать микрополярные волны, а также, что такое поступание создает возможность проверки микрополярной теории упругости.

1. Introduction

ALTHOUGH the literature of the past two decades is replete with the results of theoretical investigations into the nature of micropolar elasticity and the effect of couple stresses on solutions to a variety of boundary value problems, very little experimental work of a corroborative character has been reported. Inasmuch as the response of a typical micropolar material to applied surface tractions must deviate very little from that predicted by the classical elasticity theory, experiments of extremely high resolution must be designed and conducted in order to detect the existence of micropolar effects. The prospects of obtaining a quantitative evaluation of the micropolar theory should attract more effort into experimental investigations of material behavior.

GAUTHIER and JAHSMAN [1] in 1975 reported on static experimental investigations conducted with a prototype micropolar elastic material especially fabricated by embedding "rigid" aluminum shot in an elastic epoxy matrix. Theoretical analysis utilizing the basic equations of micropolar elasticity showed that the six material moduli, λ, μ, $\varkappa$, α, β, and γ, the first two being the classical Lamé constants, can be determined by means of the solutions to selected boundary value problems which model a series of simple static experiments. Specifically, these problems are the axisymmetric loading of a solid cylinder in tension and in torsion, and the cylindrical bending of a rectangular flat plate. In these examples the micropolar theory predicts an increase in specimen stiffness per unit area as the size of the specimen is reduced. Accordingly, tension and torsion tests were conducted on cylinders of different sizes and displacements were measured by both mechanical and optical means. No specimen size effect could be observed within experimental scatter and it was concluded that the experiments lacked the resolution necessary to identify micropolar behavior.

In the present work the authors have turned to a dynamic approach in which wave propagation through classical and micropolar elastic media is measured and compared. This investigation was prompted by the availability of a Kolsky apparatus in which the distortion of a stress wave is recorded as it passes axially through a short cylindrical specimen. Although the apparatus produces basically one-dimensional waves, two-dimensional waves may be generated in the specimen. To assist in the interpretation of the experimental data, an analysis was carried out on a micropolar counterpart to the Rayleigh-Lamb infinite plate problem in plane strain. The plate geometry was selected in preference to the cylinder geometry because of its mathematical tractability when compared to the Pochhammer–Chree problem.

The infinite plate problem for wave propagation in plane strain was first solved by RAYLEIGH [2] and LAMB [3] in 1889. LAMB [4] further elaborated on the plate problem in 1917 by studying higher vibrational modes and performing numerical calculations to display graphically the frequency vs. wave number curves. It remained for the general availability of digital computers in the 1950's to permit the unraveling of the various modes of the frequency equation. The frequency spectrum was studied in great detail by MINDLIN and his associates, and a general mapping of the frequency and dispersion curves is provided in [5] and [6]. Further discussion appears in ACHENBACH [7].

The plane wave propagation problem in a micropolar elastic half-space is treated by ERINGEN [8] for a traction-free boundary, and by NOWACKI and NOWACKI [9] for the case with surface tractions. ACHENBACH [10] deals with waves in a micropolar plate by an asymptotic method. NOWACKI and NOWACKI [11] also analyze the micropolar plate problem in plane strain but include vibrational modes.

The analysis and experiments, and the conclusions drawn therefrom are detailed in the sections which follow.

2. Analysis

The plane strain problem for the infinite plate is formulated as follows. We consider all motions to be restricted to the $x-y$ plane, Fig. 1, and wave propagation to be directed in the positive x-direction of a plate whose thickness is $2h$. Only distributions symmetric

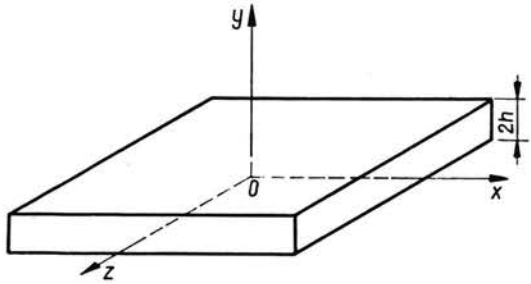

FIG. 1. Infinite plate coordinates.

to the x-axis will be treated in this development. The procedure and notation used will be similar to that of ERINGEN [8] for the half-space. For the case of plane strain the only displacements are u and v corresponding to the x- and y-directions, and the only microrotation component is Φ_z parallel to the z-axis. The boundaries $y = \pm h$ are traction-free. The basic equations of micropolar elasticity under these conditions reduce as follows:

Field equations

$$
\begin{aligned}
&(\lambda+\mu)\frac{\partial}{\partial x}\left(\frac{\partial u}{\partial x}+\frac{\partial v}{\partial y}\right)+(\mu+\varkappa)\nabla^2 u+\varkappa\frac{\partial \Phi_z}{\partial y}-\varrho\frac{\partial^2 u}{\partial t^2}=0,\\
&(\lambda+\mu)\frac{\partial}{\partial y}\left(\frac{\partial u}{\partial x}+\frac{\partial v}{\partial y}\right)+(\mu+\varkappa)\nabla^2 v-\varkappa\frac{\partial \Phi_z}{\partial x}-\varrho\frac{\partial^2 v}{\partial t^2}=0,\\
&\gamma\nabla^2\Phi_z+\varkappa\left(\frac{\partial v}{\partial x}-\frac{\partial u}{\partial y}\right)-2\varkappa\Phi_z-\varrho j\frac{\partial^2 \Phi_z}{\partial t^2}=0.
\end{aligned}
\tag{2.1}
$$

Constitutive equations

$$
t_{yy}=\lambda\frac{\partial u}{\partial x}+(\lambda+2\mu+\varkappa)\frac{\partial v}{\partial y},
\tag{2.2}
$$

(2.2) [cont.]
$$t_{yx} = \mu \frac{\partial v}{\partial x} + (\mu + \varkappa) \frac{\partial u}{\partial y} + \varkappa \Phi_z,$$
$$m_{yz} = \gamma \frac{\partial \Phi_z}{\partial y}.$$

Boundary conditions

(2.3)
$$t_{yy}(\pm h) = t_{yx}(\pm h) = m_{yz}(\pm h) = 0.$$

In the above ϱ is the material density, j is the spin inertia, t is time, t_{ij} are the components of the asymmetric stress tensor, and m_{ij} the components of the couple stress tensor.

For symmetric motion, the solutions are

(2.4)
$$u = A\cosh \zeta y e^{i\xi(x-ct)},$$
$$v = B\sinh \zeta y e^{i\xi(x-ct)},$$
$$\Phi_z = C\sinh \zeta y e^{i\xi(x-ct)},$$

where ξ is the wave number along x, ζ is the wave number along y, c is the wave speed, and A, B, and C are integration constants. The wave numbers and wave speed may be real or imaginary (more generally complex). Therefore, the solutions may be either periodic or local in space, and periodic or transient in time. By substitution of Eqs. (2.4) into Eqs. (2.1) the field equations are converted to

(2.5)
$$[(c_1^2+c_3^2)\xi^2-(c_2^2+c_3^2)\zeta^2-\xi^2c^2]A-(c_1^2-c_2^2)i\xi\zeta B-c_3^2\zeta C = 0,$$
$$(c_1^2-c_2^2)i\xi\zeta A+[(c_1^2+c_3^2)\zeta^2-(c_2^2+c_3^2)\xi^2+\xi^2c^2]B-c_3^2 i\xi C = 0,$$
$$\frac{c_3^2}{c_2^2}\zeta A-\frac{c_3^2}{c_2^2}i\xi B-j\left[\frac{c_4^2}{c_2^2}(\zeta^2-\xi^2)-2\frac{c_3^2}{jc_2^2}+\frac{\xi^2c^2}{c_2^2}\right]C = 0,$$

where

(2.6)
$$c_1^2 = \frac{\lambda+2\mu}{\varrho}, \quad c_2^2 = \frac{\mu}{\varrho}, \quad c_3^2 = \frac{\varkappa}{\varrho}, \quad c_4^2 = \frac{\gamma}{\varrho j},$$
$$\varepsilon = \frac{c_3^2}{c_2^2} = \frac{\varkappa}{\mu}, \quad \theta = \frac{c_4^2}{c_2^2} = \frac{\gamma}{\mu j}.$$

A nontrivial solution for A, B, and C exists only if the determinant of their coefficients vanishes. Upon substitution of the last two equations of the set (2.6), we obtain for this determinant

(2.7)
$$\left\{\left[j\theta\zeta^2-j\left(\theta-\frac{c^2}{c_2^2}\right)\xi^2-2\varepsilon\right]\left[(1+\varepsilon)\zeta^2-\left(1+\varepsilon-\frac{c^2}{c_2^2}\right)\xi^2\right]+\varepsilon^2(\zeta^2-\xi^2)\right\}$$
$$\times\left[\left(\varepsilon+\frac{c_1^2}{c_2^2}\right)\zeta^2-\left(\varepsilon+\frac{c_1^2-c^2}{c_2^2}\right)\xi^2\right] = 0.$$

It is reasonable to assume that the micropolar modulus $\varkappa$ is very much smaller than the classical Lamé constant μ such that $\varepsilon \ll 1$, and $O(\varepsilon^2)$ terms can be neglected [8]. With this linearization the roots of Eq. (2.7) are

$$\zeta_1^2 = \left(1 - \frac{c^2}{c_1^2 + \varepsilon c_2^2}\right)\xi^2,$$

$$\zeta_2^2 = \left[1 - (1-\varepsilon)\frac{c^2}{c_2^2}\right]\xi^2, \tag{2.8}$$

$$\zeta_3^2 = 2\frac{\varepsilon}{j\theta} + \left(1 - \frac{c^2}{\theta c_2^2}\right)\xi^2.$$

Since $\cosh\zeta y = \cosh(-\zeta y)$ and $\sinh\zeta y = -\sinh(-\zeta y)$, the $\pm$ roots of ζ_k $(k = 1, 2, 3)$ can be combined to obtain in place of Eqs. (2.4) the series solutions

$$u = \sum_{k=1}^{3} A_k \cosh\zeta_k y e^{i\xi(x-ct)},$$

$$v = \sum_{k=1}^{3} B_k \sinh\zeta_k y e^{i\xi(x-ct)}, \tag{2.9}$$

$$\Phi_z = \sum_{k=1}^{3} C_k \sinh\zeta_k y e^{i\xi(x-ct)}.$$

This form of the solution can be further refined to

$$u = \sum_{k=1}^{3} A_k \cosh\zeta_k y e^{i\xi(x-ct)},$$

$$v = \sum_{k=1}^{3} \lambda_k A_k \sinh\zeta_k y e^{i\xi(x-ct)}, \tag{2.10}$$

$$\Phi_z = \mu_3 A_3 \sinh\zeta_3 y e^{i\xi(x-ct)},$$

where

$$\lambda_1 = \frac{\zeta_1}{i\xi}, \quad \lambda_2 = \frac{\xi}{i\zeta_2}, \quad \lambda_3 = \frac{\xi}{i\zeta_3},$$

$$\mu_3 = \frac{1}{\varepsilon\zeta_3}\left[(1+\varepsilon)\left(\frac{\xi^2 c^2}{\theta c_2^2} - \frac{2\varepsilon}{j\theta}\right) - \frac{\xi^2 c^2}{c_2^2}\right], \tag{2.11}$$

λ_1 is found by eliminating A and B in Eqs. (2.5) and using Eq. $(2.8)_1$ λ_2 and λ_3 are found by eliminating C in Eqs. $(2.5)_{1,2}$ and using Eqs. $(2.8)_{2,3}$. Letting $\mu_3 = C_3/A_3$, we obtain its value from Eq. $(2.5)_1$.

Equations (2.3) and (2.2) give on the stress-free boundary $y = \pm h$, where Eqs. (2.6) are used,

$$(c_1^2 - 2c_2^2)\frac{\partial u}{\partial x} + (c_1^2 + \varepsilon c_2^2)\frac{\partial v}{\partial y} = 0,$$

$$\frac{\partial v}{\partial x} + (1+\varepsilon)\frac{\partial u}{\partial y} + \varepsilon\Phi_z = 0, \tag{2.12}$$

$$\frac{\partial \Phi_z}{\partial y} = 0.$$

We introduce the ratios

$$k = c_2^2/c_1^2, \quad p = c^2/c_2^2, \tag{2.13}$$

which we use with Eqs. (2.11) after substituting Eqs. (2.10) into Eqs. (2.12) to obtain

$$\begin{aligned}
&\left[\left(\frac{1}{k}+\varepsilon\right)\frac{\zeta_1^2}{\xi^2}-\frac{1}{k}+2\right]\cosh(\zeta_1 h)A_1+(2+\varepsilon)\cosh(\zeta_2 h)A_2 \\
&\qquad +(2+\varepsilon)\cosh(\zeta_3 h)A_3 = 0, \\
&(2+\varepsilon)\zeta_1\sinh(\zeta_1 h)A_1+\left(\frac{\xi^2}{\zeta_2^2}+1+\varepsilon\right)\zeta_2\sinh(\zeta_2 h)A_2 \\
&\qquad +\left(\frac{\xi^2}{\zeta_3^2}+1+\varepsilon+\frac{\varepsilon\mu_3}{\zeta_3}\right)\zeta_3\sinh(\zeta_3 h)A_3 = 0, \\
&\mu_3\zeta_3\cosh(\zeta_3 h)A_3 = 0.
\end{aligned} \tag{2.14}$$

In order that A_1, A_2, and A_3 be nonzero, it is necessary for the determinant of their coefficients to vanish. This leads to

$$\begin{aligned}
&\left[\left(\frac{1}{k}+\varepsilon\right)\frac{\zeta_1^2}{\xi^2}-\frac{1}{k}+2\right]\left(\frac{\xi^2}{\zeta_2^2}+1+\varepsilon\right)\zeta_2\cosh(\zeta_1 h)\sinh(\zeta_2 h) \\
&\qquad -(2+\varepsilon)^2\zeta_1\sinh(\zeta_1 h)\cosh(\zeta_2 h) = 0.
\end{aligned} \tag{2.15}$$

We note that Eqs. $(2.8)_{1,2}$ with the aid of Eqs. (2.13) can be written as

$$\frac{\zeta_1^2}{\xi^2} = 1-\frac{p}{1/k+\varepsilon}, \quad \frac{\zeta_2^2}{\xi^2} = 1-(1-\varepsilon)p, \tag{2.16}$$

which, when used in Eq. (2.15) will yield, after some manipulation,

$$\frac{\tanh\zeta_2 h}{\tanh\zeta_1 h} = \frac{4(1+\varepsilon)\xi^2\zeta_1\zeta_2}{\left(\xi^2+\dfrac{\zeta_2^2}{1-\varepsilon}\right)^2}, \tag{2.17}$$

where the ε^2 terms are dropped. This is the micropolar counterpart of the LAMB [4] frequency equation. If $\varepsilon = 0$, the classical form is recovered.

The analysis of the frequency spectrum is facilitated by introducing $m = \zeta_2/\zeta_1$ and converting Eq. (2.17) to

$$\frac{\tanh m\zeta_1 h}{\tanh\zeta_1 h} = \frac{4(1+\varepsilon-p)}{m(2+\varepsilon-p)^2}, \tag{2.18}$$

where an alternate expression for m is

$$m^2 = \frac{1-(1-\varepsilon)p}{1-\dfrac{p}{1/k+\varepsilon}}. \tag{2.19}$$

It can be seen from Eqs. (2.13) that p is real. Inspection of Eqs. (2.16) will reveal the character of the wave numbers as follows:

Range	ξ	ζ_1	ζ_2	m
$p \leqslant (1-\varepsilon)^{-1}$	real(1)	r	r	r
	imag.	i	i	r
$(1-\varepsilon)^{-1} < p \leqslant k^{-1}+\varepsilon$	r	r	i	i
	i	i	r	i
$k^{-1}+\varepsilon < p$	r	i	i	r
	i	No solutions exist		

The micropolar Poisson's ratio is defined [1] in terms of the fundamental constants by

$$\nu_m = \frac{\lambda}{2\lambda+2\mu+\varkappa}, \tag{2.20}$$

from which

$$k = \frac{1-2\nu_m}{2-(2-\varepsilon)\nu_m}. \tag{2.21}$$

For a chosen ν_m and ε, the roots $\zeta_1 h$ of the frequency equation (2.18) are found for selected values of p making use of Eqs. (2.19) and (2.21). Equations (2.16) provide corresponding values of ξ. A dimensionless wave number $\tilde{\xi}$ and dimensionless frequency $\tilde{\omega}$ are defined by

$$\tilde{\xi} = 2\xi h/\pi, \quad \tilde{\omega} = \tilde{\xi} c\left(\frac{G_m}{\varrho}\right)^{-1/2} = \tilde{\xi}\left(\frac{p}{1+\varepsilon/2}\right)^{1/2}, \tag{2.22}$$

where $G_m = \mu+\varkappa/2 = \mu(1+\varepsilon/2)$ is the micropolar shear modulus. These parameters are the coordinates for mapping the various branches which constitute the solution of Eq. (2.17). The values of $\tilde{\xi}$ extend the full range of complex numbers, but only positive real and imaginary values will be considered here. The imaginary values of $\tilde{\omega}$ will be disregarded as they represent transient motions, neither vibrations nor propagating waves, and are of no particular interest. One exception is presented in the Appendix.

The intercepts of the branches at $\tilde{\xi} = 0$ are called *cutoff frequencies*. These values may be found by writing Eq. (2.18) for $p > 1/k+\varepsilon$

$$\frac{\tan m\zeta_1 h}{\tan \zeta_1 h} = \frac{4(1+\varepsilon-p)}{m(2+\varepsilon-p)^2}.$$

As $p \to \infty$, $m = [(1-\varepsilon)/k+\varepsilon]^{1/2}$

$$\frac{\tan m\zeta_1 h}{\tan \zeta_1 h} = 0.$$

Then, using Eqs. (2.16) and (2.22), we obtain the cutoff frequencies as

$$\zeta_1 h = n\pi/m, \quad \tilde{\omega} = (1+\varepsilon/4)n \quad (n = 2, 4, 6, \ldots), \tag{2.23}$$

or

$$\zeta_1 h = n\pi/2, \quad \tilde{\omega} = \left(\frac{2-2\nu_m}{1-2\nu_m}\right)^{1/2} n \quad (n = 1, 3, 5, \ldots). \tag{2.24}$$

(1) The lower limit of p is found by solving Eq (2.27) to follow.

Equation (2.23) gives the infinitely long wavelength frequencies for symmetric equivoluminal modes and Eq. (2.24) for the dilatational modes. It is interesting to note that the equivoluminal modes do not depend on Poisson's ratio, and the dilatational modes do not depend on the micropolar constant. It can be seen from Eqs. (2.22) that the fundamental mode passes through the origin regardless of the micropolar constant ε.

This last statement is extremely significant to the present work. The Kolsky apparatus produces a long wavelength stress wave and the fundamental mode predominates. Phase velocity measurements with a micropolar specimen should not reveal a micropolar effect.

Long waves

As the wavelength increases without bound, ξ and ζ_1 approach zero and the hyperbolic tangents in Eq. (2.17) can be replaced by their arguments,

$$\frac{\zeta_2 h}{\zeta_1 h} = \frac{4(1+\varepsilon)\xi^2\zeta_1\zeta_2}{\left(\xi^2+\dfrac{\zeta_2^2}{1-\varepsilon}\right)^2}.$$

This reduces to

$$p = \frac{4(1-k)+2\varepsilon}{1+k\varepsilon}. \tag{2.25}$$

Using Eq. (2.21) and the definitions of k and G_m, we obtain

$$p = \frac{2}{1-\nu_m}\left(\frac{2+2\varepsilon}{2+\varepsilon}\right) = c^2\left(\frac{\mu}{\varrho}\right)^{-1} = c^2\varrho\left(\frac{1+\varepsilon/2}{G_m}\right),$$
$$c = \left[\left(\frac{2}{1-\nu_m}\right)\left(\frac{G_m}{\varrho}\right)\right]^{1/2}. \tag{2.26}$$

Equation $(2.26)_2$ does not contain ε explicitly. G_m and ν_m are mechanical properties in which ε is inherent. But their direct measurement using conventional techniques does not expose the presence of ε. This is the fundamental mode of longitudinal wave propagation in a micropolar solid, and we see that the phase velocity measured in a long wavelength experiment will not differ from that predicted by the classical theory.

Short waves (Rayleigh waves)

In the case of short wavelength propagation $\zeta_{1,2}h \gg 1$ and $\tanh\zeta_{1,2}h \simeq 1$. Equation (2.17) becomes

$$4(1-\varepsilon)\xi^2\zeta_1\zeta_2 = \left(\xi^2+\frac{\zeta_2^2}{1-\varepsilon}\right)^2$$

which expands to

$$p^3-4(2+\varepsilon)p^2+8[(1+\varepsilon)(3-2k)+2k^2\varepsilon]p-16[(1+2\varepsilon)(1-k)+k^2\varepsilon] = 0. \tag{2.27}$$

The classical result is recovered by letting $\varepsilon = 0$. As an example we let $\nu_m = 1/4$, $k = [3(1+\varepsilon/4)]^{-1}$. Equation (2.27) reduces to

$$p^3-4(2+\varepsilon)p^2+\frac{28}{9}(6+7\varepsilon)p-\frac{4}{9}(24+55\varepsilon)=0.$$

A real root of this equation is

$$p = 0.8453(1+1.4441\varepsilon) = c^2\left(\frac{\mu}{\varrho}\right)^{-1} = c^2\varrho\left(\frac{1+\varepsilon/2}{G_m}\right),$$

(2.28)

$$c = 0.9194(1+0.4721\varepsilon)\left(\frac{G_m}{\varrho}\right)^{1/2}.$$

For the classical case where ε vanishes and $G_m = \mu$, the Lamb solution is recovered. Equation $(2.28)_2$ shows that a short wavelength experiment which measures the surface wave speed c will determine the micropolar constant ε where G_m has been found from a static experiment.

The roots of Eq. (2.18) are plotted in Fig. 2. The trajectories for real wave numbers are propagating waves and those for imaginary wave numbers represent localized vibra-

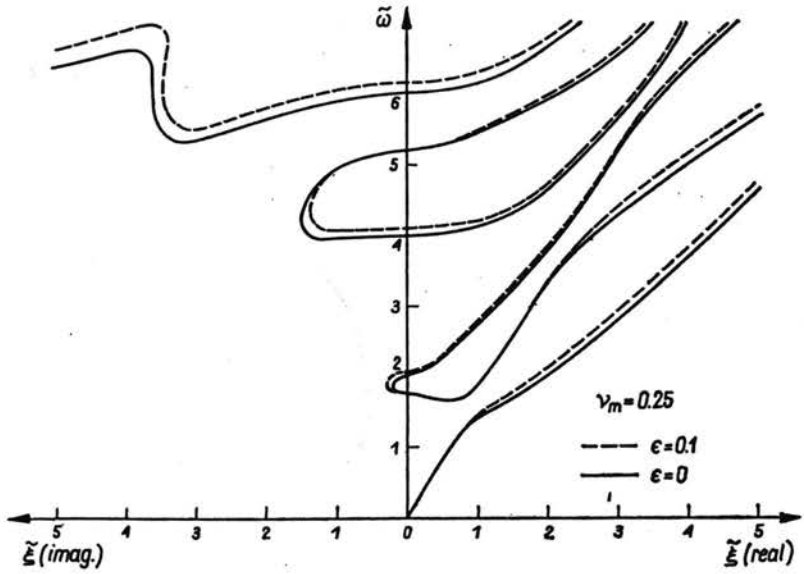

FIG. 2. Frequency spectrum of an infinite plate; classical $\varepsilon = 0$, and micropolar $\varepsilon = 0.1$; $\nu_m = 0.25$.

tions. No attempt is made to plot complex branches. Except for different Poisson's ratios, the classical results compare directly to those of MINDLIN for symmetric modes [6]. Also shown are the corresponding micropolar branches for $\varepsilon = 0.1$, and it is seen that appreciable micropolar deviation along the dilatational branches does not appear until the wave number increases past unity.

In addition to the Rayleigh–Lamb results, we have a solution for which there is no classical counterpart. This is provided by Eq. $(2.14)_3$, which also satisfies the determinantal equation if

$$\mu_3\zeta_3\cosh\zeta_3 h = 0. \tag{2.29}$$

First, we consider the possibility

$$\mu_3 \zeta_3 = \frac{1}{\varepsilon}\left[(1+\varepsilon)\left(\frac{\xi^2 c^2}{\theta c_2^2} - \frac{2\varepsilon}{j\theta}\right) - \frac{\xi^2 c^2}{c_2^2}\right] = 0.$$

This can be rearranged by using Eqs. (2.22) to give

$$\tilde{\omega}^2 = \left(\frac{2h}{\pi}\right)^2 \left(\frac{1+\varepsilon/2}{1+\varepsilon-\theta}\right)\frac{2\varepsilon}{j} = \text{constant}.$$

It has been shown by PARFITT and ERINGEN [12] that $\theta \geqslant 1+\varepsilon$, $c_4^2 \geqslant c_2^2 + c_3^2$. Therefore, $\tilde{\omega}$ is imaginary, and the corresponding motions are transient. Equation (2.29) can be written in the alternate form

$$\left[\left(1+\varepsilon-\frac{c_4^2}{c_2^2}\right)\frac{\xi^2 c^2}{c_2^2} - (1+\varepsilon)\frac{2\varepsilon}{j}\right]\cos i\zeta_3 h = 0. \tag{2.30}$$

We see immediately the coupling between shear waves c_2 and microrotation waves c_4. This coupling is retained if we allow the second factor in Eq. (2.30) to vanish,

$$i\zeta_3 h = \frac{n\pi}{2}, \quad \zeta_3^2 = -\left(\frac{n\pi}{2h}\right)^2 \quad (n = 1, 3, 5, \ldots). \tag{2.31}$$

Substitution into Eq. $(2.8)_3$ using Eqs. (2.6) gives us

$$\frac{\omega^2}{c_4^2} = \frac{2c_3^2}{jc_4^2} + \left(\frac{n\pi}{2h}\right)^2 + \xi^2,$$

where $\omega = \xi c$ is the circular frequency. For the long wavelength case, $\xi \to 0$, and

$$\frac{\omega^2}{c_4^2} = \frac{2c_3^2}{jc_4^2} + \left(\frac{n\pi}{2h}\right)^2 \quad (n = 1, 3, 5, \ldots). \tag{2.32}$$

We will make good use of this equation later.

3. Experimental measurements

The conventional Kolsky apparatus (split Hopkinson pressure bar) has been used successfully for some years to produce a nearly uniaxial stress wave for the determination of dynamic compressive, tensile, and shear properties of a variety of materials. Experience gained with equipment located in the Dynamic Material Behavior Laboratory at the University of Colorado suggested a test program of observation of wave form and speed characteristics as stress waves propagate through a micropolar elastic specimen. It was hoped that these measurements would provide a means of detecting micropolar behavior and evaluating one or more of the additional elastic constants predicted by the micropolar theory.

The essential features of the Kolsky apparatus are shown in Fig. 3. A short cylindrical specimen measuring 38.1 mm diameter by 12.7 mm long is located axially between two steel bars each 38.1 mm diameter by 914 mm long. A steel impactor 38.1 mm diameter and 50.8 mm long is accelerated by an air gun to a predetermined velocity which is measur-

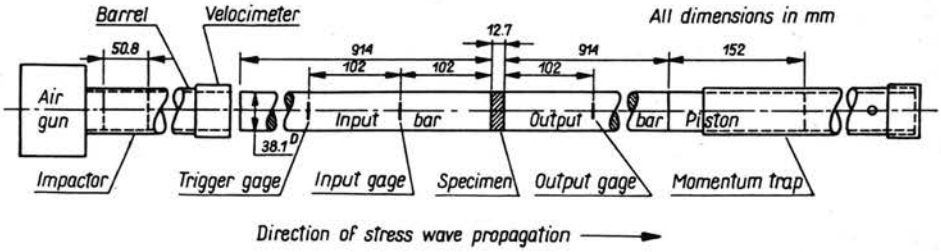

FIG. 3. Schematic arrangement of Kolsky apparatus.

ed by an optical velocimeter just before impact. Pairs of diametrically opposed semiconductor strain gages are located at distances of 102 mm from the ends of the bars in contact with the specimen. These are mounted circumferentially, with the narrow dimension in the direction of wave travel so as to assure minimum integration of the signal over the gage length. These gages provide circumferential strain histories associated with the input and output stress waves. Although a rectangular pulse is initiated by the impactor, dispersion in the input bar smooths this pulse to a bell-shaped form by the time it reaches the input gages. In the distance of 204 mm between input and output gages in the absence of a specimen (bar to bar) there is very little further change in the wave form, and any signal attenuation can be corrected for in the data obtained with test specimens.

The input and output signals are processed through conventional balancing circuits and fed to a dual channel digital storage oscilloscope. The oscilloscope is externally triggered by another pair of strain gages mounted on the input bar 102 mm ahead of the input gages. The oscilloscope displays the two wave traces both graphically and digitally. A final feature of the Kolsky apparatus is the momentum trap. This comprises a 36.5 mm diameter by 152 mm long steel piston in an air cylinder located at the far end of the output bar. The cylinder is fitted with an air bleed orifice so that the device acts as a pneumatic shock absorber. The momentum trap assures that energy transmitted into the output bar is captured before separation begins at the piston/bar interface. Further details of construction and performance of the Kolsky apparatus are given by BHUSHAN and JAHSMAN [13].

Calibration of the stress measuring system was accomplished by placing either the input or output bar, strain gages and circuitry attached, in a 1.33 MN capacity Baldwin testing machine and applying a static axial compressive load. An extremely linear correlation between strain gage signal and axial stress was obtained. This calibration obviated the need for applying a gage factor and converting tangential strain to axial stress through the two-dimensional Hooke's law.

A special man-made micropolar material was fabricated by casting a 1.4 mm diameter pure aluminum shot close-packed in an epoxy matrix. The volume fraction of aluminum was 60 percent. Specimens were carefully machined to provide flat and parallel faces for best contact with the input and output bars. Uniformity of results among several different specimens was improved by applying a static compressive preload to a stress level of 68.9 MPa in an 89.0 kN Instron testing machine. This operation served also to determine the static modulus of elasticity E_m of the micropolar material, and it was found to be

5.31 GPa. Although this is not the conventional measurement technique for obtaining the modulus of elasticity, it did match the loading conditions under which the dynamic tests would be conducted. Specimens of identical dimension were prepared also from pure epoxy and from 2024T351 aluminum alloy. Since these materials are the constituent parts of the micropolar specimens, they serve as measures for comparison of the experimental results.

All test specimens were lightly lubricated with a high-vacuum grease as they were positioned in the Kolsky apparatus. The grease serves two purposes; it provides antifriction contact with the loading bars permitting relatively unconstrained radial displacement in the specimen for one-dimensional stress as the wave passes through, and it tends to fill any voids at the interfaces due to misalignment or lack of flatness in either specimen or bars. An impactor velocity of 12 ms^{-1} was found to be optimum. It was sufficient to

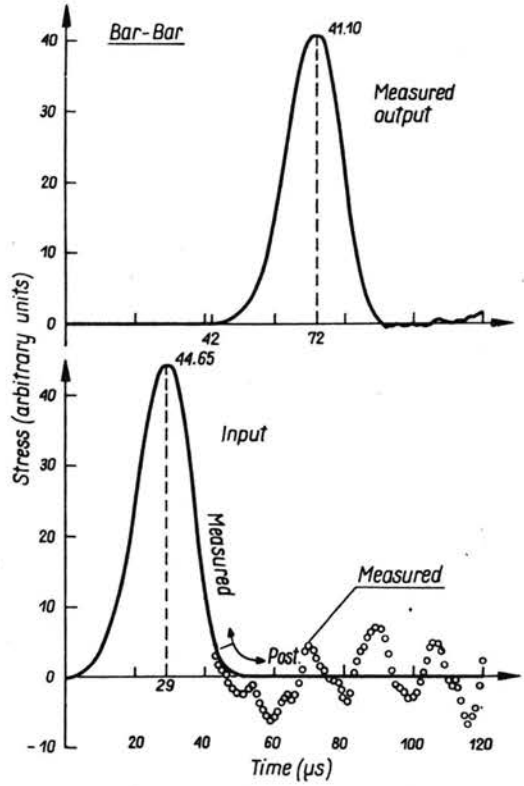

FIG. 4. Input and output oscillograms; no specimen (bar-bar).

give resolvable stress levels in the most resilient material, epoxy, yet not so high as to cause unacceptable damage to the other specimen materials.

The first test was performed without a specimen (input and output bars in contact) in order to obtain a base form and speed for the apparatus. The input and output bar traces are shown in Fig. 4 where the ordinate scale is in arbitrary stress units which convert to 5.79 MPa per division, positive values representing compressive stress. The abscissa

is the time scale in μs. The measured time lapse of 43 μs between input and output peaks over a distance of 204 mm gives a bar speed of 4.74 mm $(\mu s)^{-1}$ for steel which agrees with that calculated from the formula for bar speed $c_b = (E/\varrho)^{1/2}$, where Young's modulus $E = 179$ GPa and density $\varrho = 8.03$ Mgm^{-3}.

The measured input signal shows the effect of noise due in part to Pochhammer-Chree ringing and generated in part as the result of bar/bar interface separation. If this noise were absent, the input pulse would terminate at about 51 μs. This postulated wave form is shown in the figure as a solid curve, and the difference between it and the measured values will be used on a proportional basis to adjust all inputs to correct for this noise.

The output trace shows an 8 percent attenuation of peak value which is due to energy loss at the interface. A corresponding increase in the output data for all tests will remove this effect. Note that the noise tail present in the input signal has been effectively filtered out at the interface and does not appear in the output signal. The output trace originates at 42 μs and virtually cuts off at about 90 μs.

4. Comparison between analysis and experiment

A ray tracing technique is used to make one-dimensional wave form predictions of input and output signals based on the elastic properties of the bars and specimens. The calculated curves are composites of signals in which the basic pulse is modified by the arrival of a succession of reflected pulses each delayed by an additional transit time twice through the specimen. These multiple reflections are conveniently displayed in a time-space $(t-x)$ diagram such as that of Fig. 5. A portion of the incident pulse d is reflected at the front face of the specimen into pulse R_1. That part which enters the specimen travels

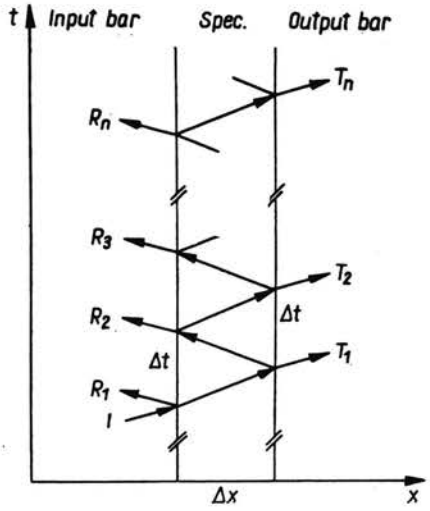

FIG. 5. Representative time vs. distance diagram depicting reflected and transmitted rays at specimen faces.

its thickness Δx to the back face where it is divided into a pulse T_1 transmitted to the output bar and a pulse reflected back to the front face where a portion returns to the input bar as R_2. This process continues for the duration of the oscilloscope record which is about 120 μs. Pulse R_1 reaches the input gages 43 μs after I. R_2 is delayed Δt depending on the wave speed c_s of the specimen. The arrival time of each successive R_n is incremented a Δt. The T_1 signal reaches the output gages at time 43 μs plus $\Delta t/2$ after detection of I by the input gages, and T_2 a Δt increment later. Tabulation of the first six R and T rays was generally sufficient to produce a suitable wave form, stress being calculated at each μs starting at time zero when the front of the input pulse appeared on the oscilloscope.

The wave speed c_b in the bars was determined experimentally by measuring the elapsed time between input and output signal peaks in a bar/bar test. This method is not reliable, however, for finding the specimen speed c_s because of the delaying effect of multiple reflections. Instead, c_s was calculated from the known or measured material properties E and ϱ. The strengths of the R and T rays relative to I are given by

$$R_1 = \frac{1-X}{1+X} I, \quad R_n = \frac{4XI}{(1+X)^2}\left(\frac{X-1}{X+1}\right)^{2n-3} \quad (n > 1),$$
$$T_n = \frac{4XI}{(1+X)^2}\left(\frac{X-1}{X+1}\right)^{2n-2}, \tag{4.1}$$

where $X = (\varrho c)_b/(\varrho c)_s$, the ratio of bar and specimen impedances. The time increment appearing in the $t-x$ diagram can be found from $\Delta t = 2\Delta x/c_s$. Table 1 lists the pertinent properties of the four materials involved in the tests. It shows that $X > 1$ for all combinations. Therefore, a reversal of sign in R_1 results in a tensile pulse being reflected back to the input gages. All other R_n and T_n are compressive.

Table 1. Material Properties (measured).

Material	E GPa	ϱ Mgm^{-3}	c kms^{-1}	$\varrho c \times 10^{-6}$ $kgm^{-2}\ s^{-1}$	X
Steel bar	*179	*8.03	4.74	38.0	—
Aluminum	*73.1	2.64	5.26	13.9	2.74
Epoxy	4.21	1.06	1.99	2.11	18.0
Micropolar	5.31	2.19	1.56	3.41	11.2

* Taken from literature.

Table 1a. Estimated Error in Table 1.

Material	E ±%	ϱ ±%	c ±%	ϱc ±%	X ±%
Steel bar	—	0.1	2.0	2.1	—
Aluminum	—	0.2	2.0	2.2	4.3
Epoxy	2.0	0.2	1.1	1.3	3.5
Micropolar	2.6	0.2	1.4	1.6	3.5

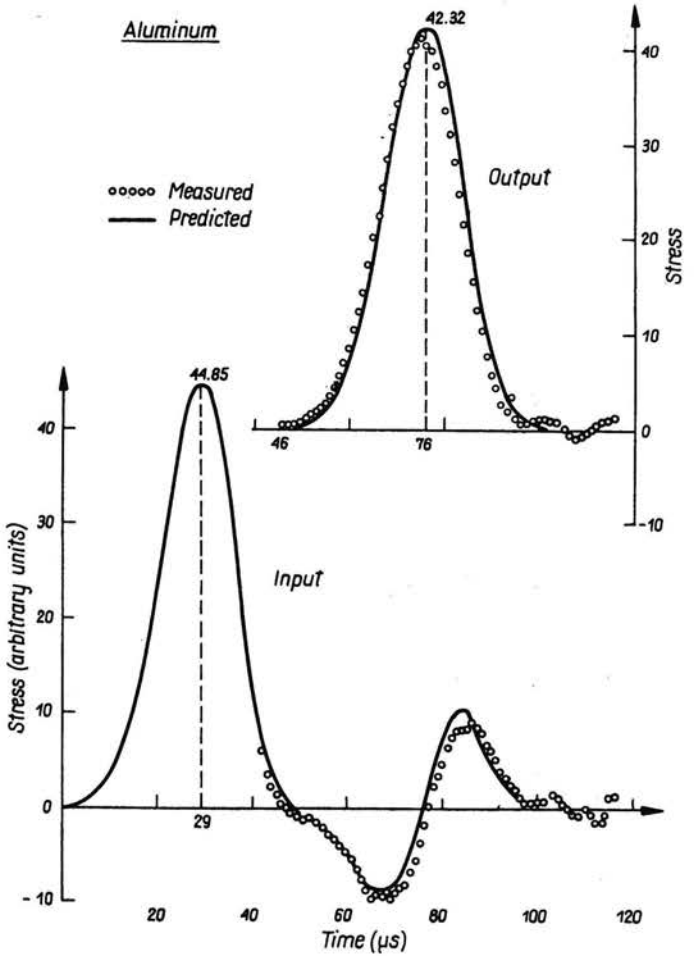

FIG. 6. Input and output oscillograms; aluminum specimen.

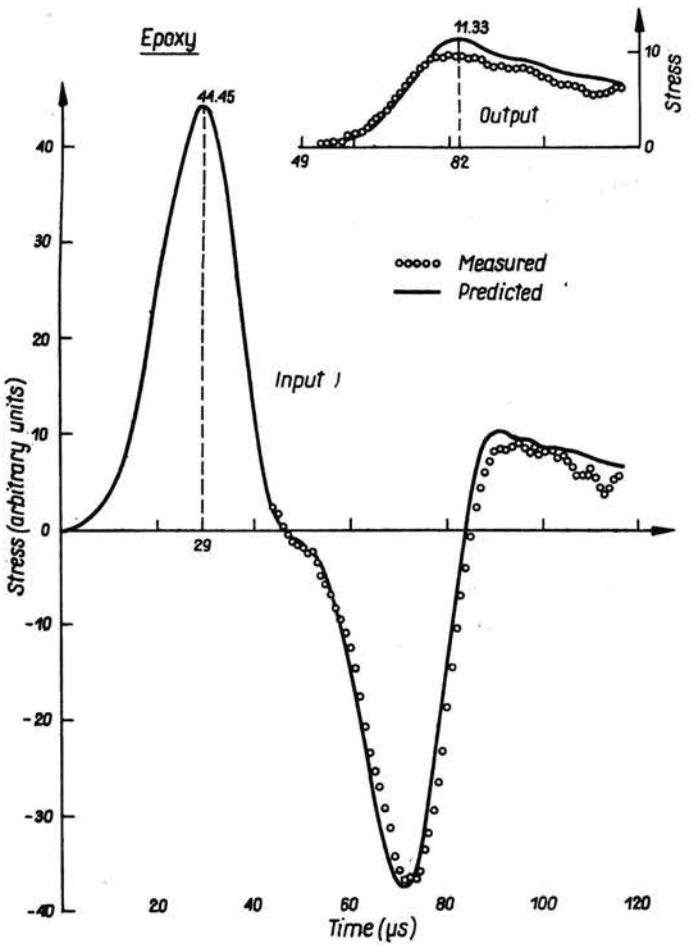

FIG. 7. Input and output oscillograms; epoxy specimen.

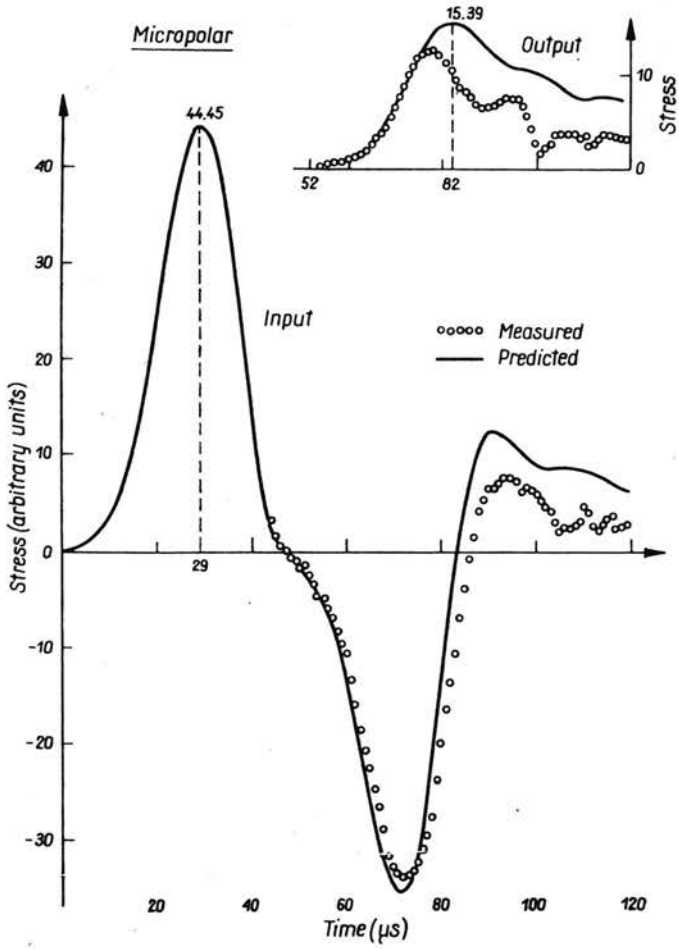

FIG. 8. Input and output oscillograms; micropolar specimen.

Typical experimental results for aluminum, epoxy, and micropolar specimens are shown in Figs. 6, 7 and 8, respectively. The measured data were corrected for interface disturbances as described in the previous section, and these points are shown by circles in the figures. The resulting traces give the best possible picture of the undistorted wave form as it is altered by normal reflections at the interfaces and by internal properties of the specimen material. The solid curves are the forms predicted from ray tracing assuming one-dimensional wave propagation.

The response of the aluminum specimen depicted in Fig. 6 shows excellent agreement between predicted and measured wave forms both in timing and magnitude. Thus, for a homogeneous elastic sample we are confident of the validity of our method of conditioning the data to eliminate interface noise, and of the usefulness of the ray tracing technique to provide a theoretical standard. Figure 7 shows good synchronization but a slight attenuation of the output signal compared to the predicted trace for epoxy. The micropolar

specimen of Fig. 8 exhibits good synchronization but anomalous ripples and considerable attenuation of signals.

Table 1a gives the estimated error of measurement of the material properties listed in Table 1. In addition, it is estimated that stress measurement is repeatable to ± 0.58 MPa with absolute value of $\pm 2\%$. Timing is to ± 1 μs. Although the strength of the predicted input and output signals is affected by the accuracy of the material wave speed determination, the timing of the trace is relatively insensitive to this parameter. A high estimate of speed advances the pulse but simultaneously emphasizes the later reflections with their associated retarding effect, thereby offsetting the initial advancement.

The test results were very repeatable with the aluminum and epoxy specimens. As many as four signatures with a given sample were stored in the oscilloscope and displayed simultaneously. Very little deviation occurred from trace to trace. It was a different matter with the micropolar material. Inspection of the front face revealed a loss of aluminum shot, giving the surface a pockmarked appearance. Subsequent tests on the same specimen resulted in further damage to the face and cumulative departure from the initial wave forms. Microscopic examination of a sectioned specimen failed to reveal any internal damage. Because of surface spalling, therefore, it was necessary to use a new specimen for each test.

5. Discussion and conclusions

It is evident from Figs. 6 and 7 that a one-dimensional ray tracing technique produces a calculated dynamic response which is in very good agreement with the recorded signals if the test specimen is made from a micro-homogeneous classical material such as aluminum or epoxy. The slight attenuation apparent in the latter stages of the epoxy traces is most likely due to a viscoelastic effect in which some of the pulse energy is being absorbed in shearing motions.

A different phenomenon appears in the micropolar case. Not only is there a considerable attenuation of the signal, but a very definite ripple is superposed on both input and output traces. This effect occurred with all micropolar specimens tested and never with aluminum or epoxy. To display this anomaly better, the stress difference (measured minus predicted) is plotted from one of the tests in Fig. 9. The resulting ripples may be resolved into two frequencies with periods of about 20 μs and 10 μs. Let us assume that these ripples are associated with the first two microrotational modes in the solution equation $(2.10)_3$

$$\Phi_z = C_n \sin\left(\frac{n\pi y}{2h}\right) e^{i\xi(x-ct)},$$

where $C_n = -i\mu_3 A_3$. We have seen in Eq. (2.30) the coupling between microrotational and shear waves. With sinusoidal thickness distributions of both Φ_z and $\partial u/\partial y$, there is every probability that the thickness-shear motions will excite microrotational modes.

With this reasoning we return to Eq. (2.32) and write

$$\frac{\omega_1^2}{c_4^2} = \frac{2c_3^2}{jc_4^2} + \left(\frac{\pi}{2h}\right)^2,$$

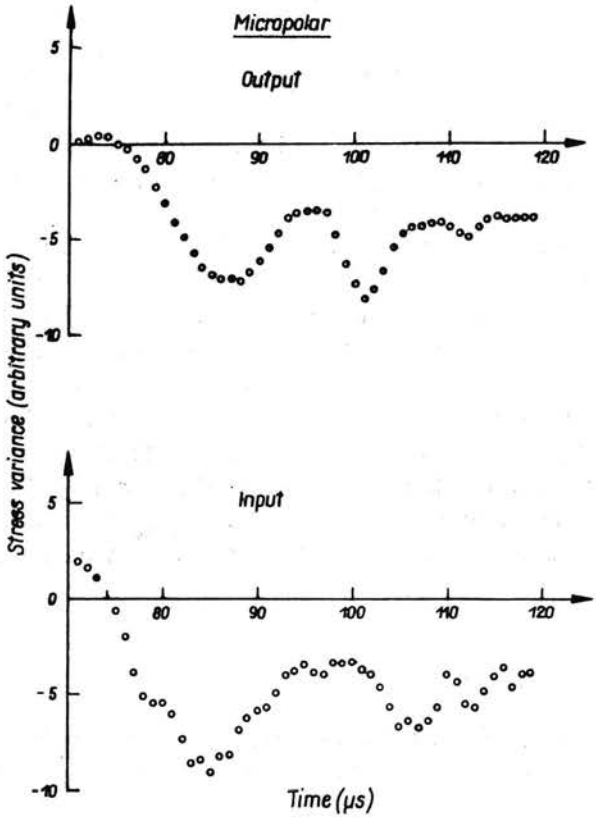

FIG. 9. Stress variance of micropolar specimen; measured value minus predicted value.

$$\frac{\omega_3^2}{c_4^2} = \frac{2c_3^2}{jc_4^2} + \left(\frac{3\pi}{2h}\right)^2,$$

from which

$$c_3^2 = j\left(\frac{9\omega_1^2 - \omega_3^2}{16}\right),$$

$$c_4^2 = \left(\frac{2h}{\pi}\right)^2\left(\frac{\omega_3^2 - \omega_1^2}{8}\right).$$

We assume the micropoles (aluminum shot) to be 1.4 mm diameter spheres. The spin inertia j (radius of gyration squared) is calculated to be 0.196 mm^2. If we associate the plate thickness with the specimen diameter, we have $2h = 38.1$ mm. Then with $\omega_n \tau_n = 2\pi$, $\tau_1 \simeq 6\pi$ μs, and $\tau_3 \simeq 3\pi$ μs, we find the micropolar wave speeds to be $c_3 = 0.0825$ mm (μs)$^{-1}$ and $c_4 = 2.48$ mm (μs)$^{-1}$.

The determination of c_3 and c_4 enables us to calculate the rest of the wave speeds and some of the micropolar elastic moduli. A measured value of $\nu_m = 0.4$ as reported in [14] is used in these calculations, and this same reference provides the relations

$$\lambda = \frac{E_m \nu_m}{(1+\nu_m)(1-2\nu_m)}, \qquad 2\mu+\varkappa = \frac{E_m}{1+\nu_m}, \tag{5.1}$$

which combine with Eqs. (2.6) to complete our calculations.

To summarize,

$$\begin{aligned} \lambda &= 7.59 \text{ GPa}, & c_1 &= 2.28 \text{ mm}(\mu\text{s})^{-1}, \\ \mu &= 1.89 \text{ GPa}, & c_2 &= 0.929, \\ \varkappa &= 14.9 \text{ MPa}, & c_3 &= 0.0825, \\ \gamma &= 2.63 \text{ kN}, & c_4 &= 2.48, \\ \varepsilon &= c_3^2/c_4^2 = \varkappa/\mu = 0.0078, \\ \theta &= c_4^2/c_2^2 = \gamma/\mu j = 7.11. \end{aligned} \tag{5.2}$$

Since our assumption that $\varepsilon \ll 1$ is correct, linearization in ε of the determinant of Eq. (2.7) to obtain the roots ζ_k of Eqs. (2.8) is justified.

We make one further interpretation of the test results. Although a slight viscoelastic attenuation is evident in the response of the pure epoxy in Fig. 7, and this effect is presumed to be present as well in the micropolar composite containing epoxy, the major loss of signal shown in Fig. 8 is caused by the transfer of energy from the axial compression wave to rotational motions of the micropoles. Direct detection of these micromotions is not possible with the present instrumentation.

The Kolsky apparatus has proven to be a useful device for producing a one-dimensional stress pulse for wave propagation studies in short cylindrical specimens. Although a rectangular pulse is initiated by the impactor of an air gun, the dispersive properties of the input bar serve to smooth the pulse which passes through the specimen. Modern strain gage instrumentation and a dual recording digital oscilloscope provide data of high resolution for the analysis of the dynamic properties of materials. Since the waves are essentially one-dimensional, it is believed that the plane strain solution of the traction-free infinite plate at small wave numbers is a suitable model for experiments with short cylinders. And the Rayleigh–Lamb equations are certainly more amenable to numerical calculations than the Pochhammer–Chree infinite cylinder solutions with their Bessel functions.

Results of the analysis and experiments reported in this work show, however, that little success can be expected from attempts to measure wave speed deviation due to micropolar effects, even with short wavelength experiments. Frequency curves show only a slight departure of a micropolar material from the classical theory, and then for a micropolar constant 13 times that of the measured value!

Instead, major efforts should be directed toward the generation and measurement of microrotational waves in prototype micropolar specimens. It has been shown that these modes do exist and are unique to a material with microstructure. The transfer of bulk translational energy to spin energy of the micropoles occurs in a wavelike fashion and can be achieved by the Kolsky apparatus and measured with instrumentation of sufficiently high resolution. It is hoped that this work will encourage further investigations into the dynamic properties of a variety of materials with microstructure. Such efforts will help to assess the importance of the micropolar elastic theory.

Appendix

A branch of the Rayleigh–Lamb frequency spectrum not reported before appears in the region of imaginary frequency and imaginary wave numbers and is plotted on $i\tilde{\omega}$-, $i\tilde{\xi}$- axes in Fig. 10. This branch does not reach the $i\tilde{\omega}$- axis, and it is found in the range

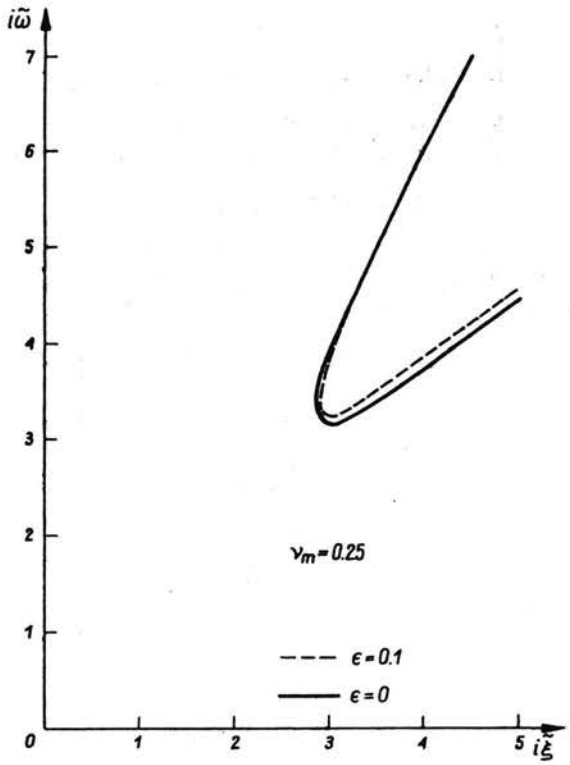

FIG. 10. Localized transient branch of frequency spectrum of infinite plate; classical $\varepsilon = 0$, and micropolar $\varepsilon = 0.1$; $\nu_m = 0.25$.

of real wave speeds $(1-e)^{-1} < p \leqslant k^{-1}+\varepsilon$. The micropolar curve which is distinct in the lower arm merges with the classical curve in the upper arm. These solutions depict localized transient motions. It is possible that this is the first of a family of such detached branches existing in the imaginary plane.

References

1. R. D. GAUTHIER, W. E. JAHSMAN, *A quest for micropolar elastic constants*, J. Appl. Mech., Trans. ASME, **97**, Series E, 369–374, 1975.
2. Lord RAYLEIGH, *On the free vibrations of an infinite plate of homogeneous isotropic elastic matter*, Proc. London Mathematical Soc., **20**, 225–234, 1889.
3. H. LAMB, *On the flexure of an elastic plate*, Proc. London Mathematical Soc., **21**, 70–90, 1890.
4. H. LAMB, *On waves in an elastic plate*, Proc. Royal Soc. of London, **93**, Series A, 114–128, 1917.

5. R. D. MINDLIN, M. A. MEDICK, *Extensional vibrations of elastic plates*, J. Appl. Mech., Trans. ASME, **81**, 562–569, 1959.
6. R. D. MINDLIN, *Waves and vibrations in isotropic, elastic plates*, in: Structural mechanics, J. N. GOODIER, and N. J. HOFF, eds., New York, Pergamon Press, 199–232, 1960.
7. J. D. ACHENBACH, *Wave propagation in elastic solids*, Amsterdam–London, North Holland Publishing Co. (American Elsevier, New York, distributor), 220–236, 1973.
8. A. C. ERINGEN, *Theory of micropolar elasticity*, in: Fracture, H. LIEBOWITZ, ed., Vol. 2, New York, Academic Press, 711–713, 1968.
9. W. NOWACKI, W. K. NOWACKI, *The plane Lamb problem in a semi-infinite micropolar elastic body*, Arch. Mech., **21**, 3, 241–260, 1969.
10. J. D. ACHENBACH, *Free vibrations of a layer of micropolar continuum*, Intern. J. Engng. Sci., **7**, 1025–1039, 1969.
11. W. NOWACKI, W. K. NOWACKI, *Propagation of monochromatic waves in an infinite micropolar elastic plate*, Bull. Acad. Polon. Sci., Série Sci. Techn., **17**, 1, 29–37, 1969.
12. V. R. PARFITT, A. C. ERINGEN, *Reflection of plane waves from the flat boundary of a micropolar elastic halfspace*, Report No. 8–3, General Technology Corp., Lafayette, Ind., 1966.
13. B. BHUSHAN, W. E. JAHSMAN, *Measurement of dynamic material behavior under nearly uniaxial strain conditions*, Intern. J. of Solids and Struc., **14**, 9, 739–754, 1978.
14. R. D. GAUTHIER, *Analytical and experimental investigations in linear isotropic micropolar elasticity*, Doctoral Dissertation, University of Colorado, 1974.

COLORADO SCHOOL OF MINES, GOLDEN, COLORADO, USA
and
UNIVERSITY OF COLORADO, BOULDER, COLORADO, USA

Received January 15, 1981.